Determination of the Ground State of Manganese Phthalocyanine in an Argon Matrix Using Magnetic Circular Dichroism and Absorption Spectroscopy

Bryce E. Williamson,*,† Thomas C. VanCott,‡,§ Michael E. Boyle,*,# G. Christian Misener,‡,⊥ Martin J. Stillman,*,∥ and Paul N. Schatz*,‡

Contribution from the Chemistry Department, University of Virginia, Charlottesville, Virginia 22901, the Chemistry Department, University of Canterbury, Christchurch 1, New Zealand, Naval Research Laboratory, Code 6123, Washington, D.C. 20375-5000, and the Chemistry Department, University of Western Ontario, London, Ontario N6A 5B7, Canada.
Received July 25, 1991

Abstract: The magnetic circular dichroism (MCD) and absorption spectra of manganese phthalocyanine isolated in an Ar matrix (MnPc/Ar) have been studied at a temperature of ~5 K over the range 10000–33000 cm^{-1}. The absorption spectrum exhibits strong, resolved bands at 11600, 15000, 16500, 19700, 20300, 22600, and 29600 cm^{-1}. The data require an orbitally degenerate ground state and are quantitatively consistent with a $^4E_g(e_g^3b_{2g}a_{1g})$ ground-state term with $g_\parallel = 8.0 \pm 0.8$. This differs from the β-phase solid where magnetic susceptibility measurements establish a $^4A_{2g}(b_{2g}^2e_g^2a_{1g})$ ground state, which is probably a consequence of intermolecular interactions. The dispersion of the MCD allows assignment of the 15000- and 16500-cm^{-1} bands respectively to a ligand-to-metal charge-transfer (LMCT) transition and the Q ($\pi \rightarrow \pi^*$) transition. This result suggests that the strongest red band in the solution spectra of MnPc, normally assigned to the Q ($\pi \rightarrow \pi^*$) transition, also contains contributions from a LMCT transition.

I. Introduction

The phthalocyanine ligand (Pc^{2-}), the dianion of tetraazatetrabenzoporphyrin) forms neutral complexes with a large number of divalent metal ions. These complexes, known collectively as the metallophthalocyanines (MPc), have found important applications in many fields of science and technology, and have given rise to a very large literature.[1]

One of the more interesting scientific applications of MPc molecules is the modeling of biologically important porphyrin-like species. In this regard, the manganese complex (MnPc) is particularly useful. The metal ion exists in several stable oxidation states depending on the number and the nature of axial ligands.[2,3] The molecule as a whole can undergo photochemical redox reactions[3,4] and has an extensive chemistry with oxygen[2-5] forming μ-oxo dimers[4,5] and an oxygen adduct believed to be a superoxide.[5] The electrochemistry of MnPc has also received a good deal of attention and is found to involve both the central metal ion and the ligand.[6,7]

For MPc molecules in solution it is very common for the solvent molecules to ligate axially with the metal ion.[2-5,7,8] For most MPc complexes (particularly those with closed-shell metal ions), such interactions have little effect on the energies of ligand-based transitions. For example, $Mn^{II}Pc$ is generally expected to show a strong $\pi \rightarrow \pi^*$ band (the Q band) near 15000 cm^{-1}, independent of solvent. However, in the presence of open-shell metals, the transition energies may be strongly dependent on both the metal oxidation state (e.g., Mn(II), Mn(III), or Mn(IV)) and spin state (low, intermediate, or high), and axial ligation can readily result in a change in one or both of these properties.[8] In addition, it is well known that when charge-transfer (CT) transitions lie close to either the Q or B bands, quite significant changes take place in the bandwidth, band energy, and band intensity.[8] In the case of MnPc, it is also clear that failure to rigorously exclude oxygen from solution results in the formation of oxo species.[2-5,8] The combination of these effects can have profound consequences for the spectra obtained from solutions of MnPc.[3,5,8-11] The effects of solvent and oxygen can be overcome to some extent by preparation of thin films by vacuum sublimation, and, as a consequence, thin film spectra do not closely resemble any of the solution spectra.[4] However, the absorption spectra obtained from such samples are subject to the effects of intermolecular interactions, which will also broaden and shift the bands relative to the spectrum of the isolated molecule.

Because of the potentially significant effects of axial ligands, solvent molecules, and solid-state interactions, no physical data previously published can be said to be representative of the isolated MnPc moiety. As a consequence, it is not even clear that the nature of the ground state of MnPc has been unambiguously identified. The earliest attempt at characterization used magnetic susceptibility measurements on β-phase solid samples[12] and suggested that MnPc is a rare example of an intermediate-spin complex with $S = {}^3/_2$, although the magnetic moment was somewhat in excess of the spin-only value. Later measurements[13-17] confirmed the spin assignment and suggest that the

† University of Canterbury.
‡ University of Virginia.
§ Present address: Walter Reed Army Institute of Research, Department of Retroviral Research, Suite 200, 13 Taft Ct, Rockville, MD 20850.
# Naval Research Laboratory.
⊥ Present address: IDEXX Corporation, 100 Fore St., Portland, ME 04101.
∥ University of Western Ontario.

(1) See, for example: *Phthalocyanines. Properties and Applications*; Leznoff, C. C., Lever, A. B. P., Eds.; VCH: New York, 1989, and references therein.
(2) Elvidge, J. A.; Lever, A. B. P. *Proc. Chem. Soc.* **1959**, 195.
(3) Engelsman, G.; Yamamoto, A.; Markham, E.; Calvin, M. *J. Phys. Chem.* **1962**, *66*, 2517-2531.
(4) Yamamoto, A.; Phillips, L. K.; Calvin, M. *Inorg. Chem.* **1968**, *7*, 847-852.
(5) Lever, A. B. P.; Wilshire, J. P.; Quan, S. K. *Inorg. Chem.* **1981**, *20*, 761-768.
(6) Clack, D. W.; Yandle, J. R. *Inorg. Chem.* **1972**, *11*, 1738-1742.
(7) Lever, A. B. P.; Minor, P. C.; Wilshire, J. P. *Inorg. Chem.* **1981**, *20*, 2550-2553.
(8) Stillman, M. J.; Nyokong, T. *Phthalocyanines. Properties and Applications*; Leznoff, C. C., Lever, A. B. P., Eds.; VCH: New York, 1989; Chapter 3, pp 133-289.
(9) Gall, C.; Simkin, D. *Can. J. Spectrosc.* **1973**, *18*, 124-127.
(10) Lever, A. B. P.; Pickens, S. R.; Minor, P. C.; Licoccia, S.; Ramaswamy, B. S.; Magnell, K. *J. Am. Chem. Soc.* **1981**, *103*, 6800-6806.
(11) Nyokong, T. Ph.D. Thesis, University of Western Ontario, London, Ontario, 1986, pp 107-111.
(12) Lever, A. B. P. *J. Chem. Soc.* **1965**, 1821-1829.
(13) Barraclough, C. G.; Martin, R. L.; Mitra, S.; Sherwood, R. C. *J. Chem. Phys.* **1970**, *53*, 1638-1642.
(14) Barraclough, C. G.; Gregson, A. K.; Mitra, S. *J. Chem. Phys.* **1974**, *60*, 962-968.
(15) Miyoshi, H. *Bull. Chem. Soc. Jpn.* **1974**, *47*, 561-565.

0002-7863/92/1514-2412$03.00/0

ground state is predominantly $^4A_{2g}$ arising from the metal-ion configuration $b_{2g}^2e_g^2a_{1g}$. To account for the high magnetic moment, higher-order spin–orbit coupling was invoked with the ^4E_g[13] or $^6A_{1g}$[14] state. Contrary to the experimental results, however, calculations[18,19] have suggested that the isolated MnPc molecule has a ^4E_g ground state, corresponding to the configuration $e_g^3a_{1g}b_{2g}$. (A further calculation by Mathur and Singh,[20] which predicts a $^2A_{2u}$ ground state, seems unrealistic).

It should be emphasized that the solid-state measurements were made on β-phase samples where the electronic state is influenced by intermolecular electrostatic (crystal-field) and magnetic interactions. In particular, there is an axial interaction of the Mn ion with the azamethine nitrogen atoms of adjacent molecules.[21,22] The exact nature of the ground state in this environment seems to be acutely sensitive to the prevailing conditions, leading, for example, to a change from $^4A_{2g}(\pm^1/_2)$ to $^4A_{2g}(\pm^3/_2)$ as the temperature is lowered from ~80 K to ~25 K.[16]

It seems possible that the disagreement between theory and experiment concerning the nature of the ground state could be due to axial interactions. In order to test this idea, it is necessary to obtain data that can be unambiguously attributed to the isolated molecule and that provide information concerning the degeneracy of the ground state. The combination of magnetic circular dichroism (MCD) and matrix-isolation techniques can provide such information and has been successfully used on a number of previous occasions in the study of MPc molecules.[8,23-26]

II. Experimental Section

Commercial MnPc (Eastman Kodak or Strem Chemicals) was heated under vacuum for up to 24 h to remove impurities. The X-ray powder diffraction pattern of a sample prepared in this manner was in close agreement with the unit-cell parameters[22] and structure factors[27] of β-phase MPc. Fourier-transform infrared (FTIR) spectra (KBr disk) indicate these samples to be predominantly β-MnPc with the presence of small and varying amounts of α-MnPc.[28]

The full procedure for matrix deposition has been described previously.[24,25] MnPc samples were sublimed from a quartz Knudsen cell and codeposited with a large excess of argon on to a cryogenically cooled c-cut sapphire window. The sublimation temperature was ~800 K, and the temperature of the deposition window was typically between 5 and 10 K.

In order to study the effects of air and oxygen on the absorption spectrum, a closed-cycle helium refrigerator (CTI-Cryogenics) operating at ~10 K was used. These spectra were obtained with a Cary-2415 spectrophotometer at a spectral resolution of 0.1 nm.

Samples for the measurement of MCD were prepared in the bore of a superconducting magnet (Oxford Instruments). Spectra were measured at a temperature of ~5 K and at magnetic fields between 0 and 3.6 T. The MCD and corresponding absorption spectrum were obtained simultaneously using a spectrometer that has been described previously.[25,29] A Hamamatsu R376 photomultiplier tube was used in the UV and visible, and a Hamamutsu R316 with S-1 response was used in the near-infrared (<14 000 cm^{-1}).

Spectra were recorded digitally and analyzed by computer. The absorbance and MCD were calibrated with standard solutions of Λ-tris-(1,2-ethanediamine)cobalt(III). Depolarization of the circularly polarized light due to the sample was determined by measuring the natural CD of a standard solution placed after the matrix and was found to be negligible.

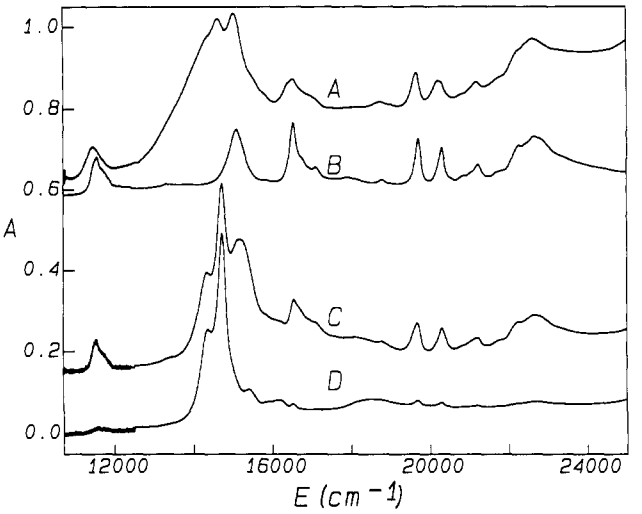

Figure 1. Absorption spectra at $T \approx 10$ K of MnPc/Ar prepared under various conditions: (A) prepared from unpurified commercial MnPc; (B) prepared from MnPc purified after several depositions; (C) purified MnPc codeposited with a small amount of air in Ar; (D) purified MnPc codeposited with 5 mol % O_2 in Ar.

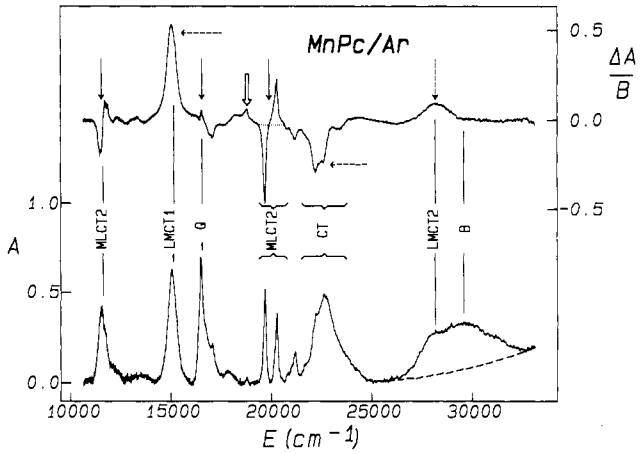

Figure 2. Absorption (A in optical density units) and MCD per tesla ($\Delta A/B$) of MnPc/Ar obtained at $T \approx 5$ K and $B = 0.15$ T. The major bands are labeled according to the assignments in section IV.5. The three solid arrows on the MCD spectrum identify bisignated $\mathscr{C}$ terms, the three dashed arrows identify prominent single-signed $\mathscr{C}$ terms, and the open boxed arrow identifies the 18 760-cm^{-1} peak used in the saturation study (Figure 3). The dashed line under the absorption above 25 000 cm^{-1}, and the dotted line in the MCD near 20 000 cm^{-1} represent base lines used for estimating $\mathscr{C}_0/\mathscr{D}_0$ values of overlapping transitions (see text).

III. Results

The absorption spectra of matrices prepared under different conditions are illustrated in Figure 1. Spectrum A was obtained after several depositions using a sample of commercial MnPc. In the Q-band region (12 500–17 500 cm^{-1}), a number of broad and strongly overlapping bands were observed. These grow at different rates during deposition and must arise from several different guest species. When further matrices were prepared using the same sample, some of these bands became progressively weaker and eventually disappeared, at which point spectrum B was obtained.

Bands appearing in spectrum A that are absent in spectrum B must be associated with impurities, at least some of which were thought to arise from surface oxidation of the MnPc crystals. To test this, matrices were prepared from the exhaustively sublimed MnPc sample in the presence of a small amount of air (spectrum C) and using 5 mol % O_2 mixed with the deposition gas (spectrum

(16) Mitra, S.; Gregson, A. K.; Hatfield, W. E.; Weller, R. R. *Inorg. Chem.* **1983**, *22*, 1729–1732.
(17) Labarta, A.; Molins, E.; Tejada, J. *Z. Phys. B* **1985**, *58*, 299–304.
(18) Schaffer, A. M.; Gouterman, M.; Davidson, E. R. *Theor. Chim. Acta* **1973**, 9–30.
(19) Maslov, V. G. *Teor. Eksp. Khim.* **1980**, *16*, 93–97.
(20) Mathur, S. C.; Singh, J. *Int. J. Quantum Chem.* **1974**, *8*, 79–82.
(21) Kirner, J. F.; Dow, W.; Scheidt, W. R. *Inorg. Chem.* **1976**, *15*, 1685–1689.
(22) Mason, R.; Williams, G. A.; Fielding, P. E. *J. Chem. Soc., Dalton Trans.* **1979**, 676–683.
(23) Bajema, L.; Gouterman, M.; Meyer, B. *J. Mol. Spectrosc.* **1968**, *27*, 225–235.
(24) VanCott, T. C.; Rose, J. L.; Misener, G. C.; Williamson, B. E.; Schrimpf, A. E.; Boyle, M. E.; Schatz, P. N. *J. Phys. Chem.* **1989**, *93*, 2999–3011.
(25) Misener, G. C. Ph.D. Thesis, University of Virginia, Charlottesville, VA, 1987.
(26) VanCott, T. C. Ph.D. Thesis, University of Virginia, Charlottesville, VA, 1989.
(27) Brown, C. J. *J. Chem. Soc. A* **1968**, 2488–2493.
(28) Sidorov, A. N.; Kotlyar, I. P. *Opt. Spectrosc.* **1961**, *11*, 92–96.
(29) Rose, J.; Smith, D.; Williamson, B. E.; Schatz, P. N.; O'Brien, M. C. M. *J. Phys. Chem.* **1986**, *90*, 2608–2615.

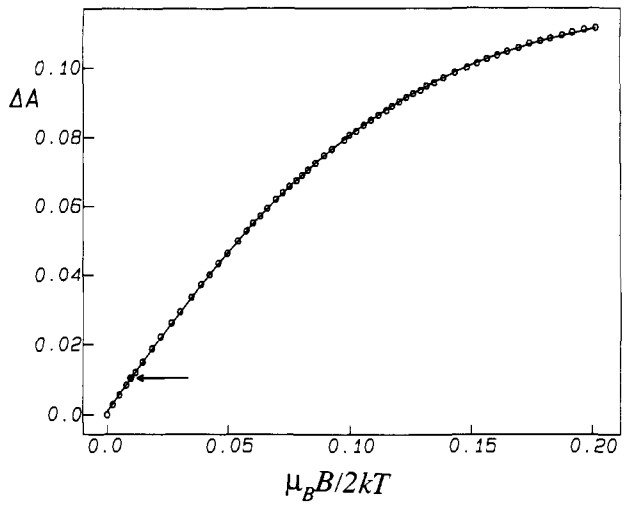

Figure 3. Magnetic saturation data (circles) for the MCD band at 18 760 cm^{-1} (open boxed arrow in Figure 2). The abscissa (units of $\mu_B B/2kT$) assumes T = 5 K and covers the range B = 0–3 T. The solid circle (see arrow) is the point obtained at B = 0.15 T, the field at which the spectra in Figure 2 were obtained. The curve through the points is the best fit obtained using eq 24 with $g_\parallel$ = 8.0 and K = 0.36. An almost identical curve is obtained using eq 23 and $g_\parallel$ = 11.5 and K = 0.26.

D). These spectra show relatively strong bands at ~14 300 and ~14 650 cm^{-1}, which are coincident with bands in spectrum A. In matrices prepared under similar conditions, the oxygen adduct $MnPcO_2$ has been identified by infrared spectroscopy,[30] and it is likely that this is the predominant impurity species. Smaller amounts of other impurities (including perhaps H_2Pc[8,31]) are probably responsible for the broad tail at the red end of the Q-band region of spectrum A.

The MCD per tesla ($\Delta A/B$) and absorption (A) spectra obtained at $T \sim 5$ K using a purified MnPc/Ar matrix are shown in Figure 2. The MCD is extremely intense, which strongly suggests the presence of $\mathcal{C}$ terms and thus ground-state degeneracy.[32] Our saturation measurements (see below) confirm this, and we have also verified that MCD amplitudes *throughout the spectrum* vary inversely with absolute temperature. Under these circumstances, it is important that the magnetic field not be too strong. First, in order to be able to apply the method of moments, spectra must be obtained in the so-called linear limit,[32] where MCD amplitudes increase linearly with magnetic-field strength. Second, the method by which we simultaneously measure the absorption and MCD[25] depends on series expansions[33] whose accuracy degrades for very large MCD signals. The spectra in Figure 2 were obtained using B = 0.15 T, in which case these errors are less than 0.3% for the ~15 000-cm^{-1} band, well within the noise level. (The errors for weaker bands are even smaller.) The saturation curve (ΔA versus B) up to B = 3.0 T for the weak, positive MCD band at ~18 760 cm^{-1} (boxed arrow in Figure 2) is shown in Figure 3. The point corresponding to B = 0.15 T is indicated by the filled circle, which is clearly within the linear region.

Two distinct types of features appear in the MCD. Examples of the first are observed near 11 600, 16 500, and 20 000 cm^{-1} (solid arrows, Figure 2) and comprise pairs of oppositely signed $\mathcal{C}$ terms. This type of dispersion is similar to that of an $\mathcal{A}$ term, and such features are sometimes described as temperature-dependent $\mathcal{A}$ terms.[32] In this work we refer to them as "bisignated" $\mathcal{C}$ terms. Features of the second type are single-signed $\mathcal{C}$ terms, and may be positive (e.g., 15 000 and 28 200 cm^{-1}) or negative (e.g., ~22 500 cm^{-1}) (dashed arrows, Figure 2).

The spectra in Figure 2 are not close in appearance to any of the earlier solution spectra.[3-5,8-11] In particular, the appearance of strong bands at both 15 000 and 16 500 cm^{-1} has not previously been reported for a monomeric MPc. However, we are confident that Figure 2 is truly representative of MnPc/Ar. Samples that were purified by heating under vacuum, and whose composition was checked by X-ray powder diffraction and FTIR spectroscopy, yield the same absorption spectrum. FTIR spectra of samples before and after deposition are identical, indicating that no decomposition occurs during sublimation. All of the MCD bands show the same temperature and field dependence, which indicates that they all arise from the same species. Finally, although the bands are sharper, the absorption spectrum in Figure 2 is similar to the thin-film spectrum of Yamamoto et al.[4]

IV. Discussion

1. Theoretical Aspects of Data Analysis. The absorbance (A) and MCD (ΔA) are defined by

$$A = (A_L + A_R)/2 \tag{1}$$

$$\Delta A = A_L - A_R \tag{2}$$

where A_L and A_R are respectively the absorbance of left and right circularly polarized light. For fully allowed transitions between Born–Oppenheimer states, the corresponding theoretical expressions are[32]

$$A/\mathcal{E} = 326.6cl\mathcal{D}_0 f(\mathcal{E}) \tag{3}$$

$$\Delta A/\mathcal{E} = 326.6\mu_B Bcl[\mathcal{A}_1(-\partial f(\mathcal{E})/\partial\mathcal{E}) + (\mathcal{B}_0 + \mathcal{C}_0/kT)f(\mathcal{E})] \tag{4}$$

Equations 3 and 4 use the rigid-shift approximation and require that the MCD be measured in the linear limit.[32] $\mathcal{E}$ is the energy (cm^{-1}) of the incident photon, $f(\mathcal{E})$ is a normalized band-shape function, μ_B is the Bohr magneton (cm^{-1} T^{-1}), and k is Boltzmann's constant (cm^{-1} K^{-1}). c and l are respectively the concentration (mol L^{-1}) and path length (cm) of the sample. $\mathcal{D}_0$ is the dipole strength of the transition, and $\mathcal{A}_1$, $\mathcal{B}_0$, and $\mathcal{C}_0$ are the corresponding Faraday parameters. $\mathcal{A}_1$ and $\mathcal{C}_0$ account for first-order Zeeman interactions within degenerate states, while $\mathcal{B}_0$ accounts for higher-order, interstate interactions.[32]

Since the MCD is completely dominated by $\mathcal{C}$ terms, we set $\mathcal{A}_1$ and $\mathcal{B}_0$ to zero in eq 4. The ratio of $\mathcal{C}_0$ to $\mathcal{D}_0$ can then be extracted from the experimental data by numerical integration.

$$\frac{\mathcal{C}_0}{\mathcal{D}_0} = \frac{kT}{\mu_B B}\frac{\int(\Delta A/\mathcal{E})\,d\mathcal{E}}{\int(A/\mathcal{E})\,d\mathcal{E}} \tag{5}$$

The integrals in eq 5 must be carried over the entire spectral envelope of the transition, which requires that the transition be well separated from others.

If the molecules are randomly oriented, then the theoretical expressions for a transition A → J are[32]

$$\bar{\mathcal{D}}_0(A\rightarrow J) = \frac{1}{3|A|}\sum_{\alpha\lambda}|\langle A\alpha|\mathbf{m}|J\lambda\rangle|^2 \tag{6}$$

$$\bar{\mathcal{C}}_0(A\rightarrow J) = \frac{-i}{3|A|}\sum_{\alpha\alpha'}\sum_{\lambda}\langle A\alpha'|\mathbf{L}+2\mathbf{S}|A\alpha\rangle\cdot(\langle A\alpha|\mathbf{m}|J\lambda\rangle\times\langle J\lambda|\mathbf{m}|A\alpha'\rangle) \tag{7}$$

In eq 6 and 7 the parameters on the left-hand side are averaged over all orientations. The matrix elements on the right-hand side pertain to zero-field states in their equilibrium nuclear configurations, with **m**, **S**, and **L** being respectively the electric-dipole, spin, and orbital angular momentum operators. α and α' are partner labels for state A, λ is a partner label for state J, and the degeneracy of A is denoted by $|A|$.

Under some circumstances MPc molecules in Ar matrices take a preferential orientation with their principal symmetry axis (z in the molecule-fixed reference frame) perpendicular to the de-

(30) Watanabe, T.; Ama, T.; Nakamoto, K. *Inorg. Chem.* **1983**, *22*, 2470–2472.
(31) Metcalf, D. H.; VanCott, T. C.; Snyder, S. W.; Schatz, P. N.; Williamson, B. E. *J. Phys. Chem.* **1990**, *94*, 2828–2832.
(32) Piepho, S. B.; Schatz, P. N. *Group Theory in Spectroscopy with Applications to Magnetic Circular Dichroism*; Wiley: New York, 1983.
(33) Collingwood, J. C.; Day, P.; Denning, R. G.; Quested, P. N.; Snellgrove, T. R. *J. Phys. E.* **1974**, *7*, 99–104.

Table I. Potentially Nonzero Electric-Dipole Transition Moments for $S = {}^3/_2 \rightarrow S = {}^3/_2$ Transitions of MnPc[a]

	$\|E_u'\alpha'\rangle$	$\|E_u'\beta'\rangle$	$\|E_u''\alpha''\rangle$	$\|E_u''\beta''\rangle$
$\langle E_g'\alpha'\|$	m_0	m_{+1}	m_{-1}	
$\langle E_g'\beta'\|$	m_{-1}	m_0		m_{+1}
$\langle E_g''\alpha''\|$	m_{+1}		m_0	m_{-1}
$\langle E_g''\beta''\|$		m_{-1}	m_{+1}	m_0

[a] $\langle A|m_{-1}|J\rangle$, $\langle A|m_0|J\rangle$, and $\langle A|m_{+1}|J\rangle$ are respectively the matrix elements for left circularly polarized, z-polarized, and right circularly polarized transitions A → J.

position window.[24,31] In this case, averaging is carried out in the x,y plane, and the expressions for $\mathcal{C}_0$ and $\mathcal{D}_0$ are modified:

$$\mathcal{D}_0^z(A\rightarrow J) = \frac{-1}{|A|}\sum_{\alpha\lambda}\langle A\alpha|m_{-1}|J\lambda\rangle\langle J\lambda|m_{+1}|A\alpha\rangle + \langle A\alpha|m_{+1}|J\lambda\rangle\langle J\lambda|m_{-1}|A\alpha\rangle \quad (8)$$

$$\mathcal{C}_0^z(A\rightarrow J) = \frac{1}{|A|}\sum_{\alpha\alpha'}\sum_{\lambda}\langle A\alpha'|L_0 + 2S_0|A\alpha\rangle(\langle A\alpha|m_{-1}|J\lambda\rangle \times \langle J\lambda|m_{+1}|A\alpha'\rangle - \langle A\alpha|m_{+1}|J\lambda\rangle\langle J\lambda|m_{-1}|A\alpha'\rangle) \quad (9)$$

The z superscripts signify that these parameters pertain to the oriented case. L_0 and S_0 are the z components of **L** and **S**, while $m_{\pm1}$ are components of **m** defined by

$$m_{\pm1} = \mp\frac{1}{\sqrt{2}}(m_x \pm im_y) \quad (10)$$

$\langle A|m_{-1}|J\rangle$ and $\langle A|m_{+1}|J\rangle$ are respectively the matrix elements for the left circularly polarized (lcp) and right circularly polarized (rcp) transitions, A → J.

The spectral region of Figure 2 should be dominated by $\pi \rightarrow \pi^*$ and CT transitions[10,34] which are predicted to be polarized in the plane of the molecule and can give rise to $\mathcal{C}$ terms. For such transitions, eqs 8 and 9 give[24]

$$\mathcal{D}_0^z = {}^3/_2\bar{\mathcal{D}}_0 \quad (11)$$

$$\mathcal{C}_0^z = 3\bar{\mathcal{C}}_0 \quad (12)$$

$$\mathcal{C}_0^z/\mathcal{D}_0^z = 2\bar{\mathcal{C}}_0/\bar{\mathcal{D}}_0 \quad (13)$$

$n \rightarrow \pi^*$ transitions are also possible. These are z-polarized, cannot give rise to $\mathcal{C}$ terms, and will be observed only if molecular orientation is incomplete or with the aid of vibronic interactions.[24] We see no evidence for such transitions and do not consider them further.

For a d^5 ion in a D_{4h} crystal field, a number of ground states are possible.[35] In the following, we consider only those states that have been suggested previously, viz., ${}^4A_{2g}$[13-17] or ${}^4E_g$.[18,19] We assume no mixing between configurations and consider Zeeman interactions only within each term. We adopt the notation $|({}^{2S+1}hM_S\theta)t\tau\rangle$ to describe a spin–orbit (SO) state that transforms as partner τ of irrep (irreducible representation) t. S is the total-spin quantum number and M_S is the corresponding magnetic quantum number. h and θ are respectively the orbital irrep and orbital partner label. For E terms, $\theta = \pm1$.

Assuming D_{4h} symmetry, $S = {}^3/_2$ spans the irreps $E_g' + E_g''$. The SO states arising from the terms ${}^4A_{2g}$ and ${}^4E_g$ are then given by the direct products of the spin and orbital irreps:

$$A_{2g}\otimes(E_g' + E_g'') = E_g' + E_g'' \quad (14)$$

$$E_g\otimes(E_g' + E_g'') = 2E_g' + 2E_g'' \quad (15)$$

Hence the lowest energy level of MnPc will transform as E_g' or E_g''. The electric-dipole operator transforms as $a_{2u} + e_u$. (We denote the irreps of operators and orbitals in lower case to distinguish them from state labels.) The allowed electric-dipole transitions are therefore $E_g' \rightarrow (E_u', E_u'')$ and $E_g'' \rightarrow (E_u', E_u'')$. The potentially nonvanishing matrix elements for such transitions are summarized in Table I. To determine the specifically allowed transitions, the results of Table I must be combined with the selection rule $\Delta M_S = 0$.

Table II. Spectroscopic Parameters for $S = {}^3/_2 \rightarrow S = {}^3/_2$ Transitions of MnPc

initial state	final state	$\bar{\mathcal{D}}_0$[a]	$\bar{\mathcal{C}}_0/\bar{\mathcal{D}}_0$[b]
	x,y-Polarized Transitions		
E_g'	E_u'	$^1/_6\|\langle E_g'\|\|m^{e_u}\|\|E_u'\rangle\|^2$	$g_\parallel(E_g')/2$
E_g'	E_u''	$^1/_6\|\langle E_g'\|\|m^{e_u}\|\|E_u''\rangle\|^2$	$-g_\parallel(E_g')/2$
E_g''	E_u'	$^1/_6\|\langle E_g''\|\|m^{e_u}\|\|E_u'\rangle\|^2$	$g_\parallel(E_g'')/2$
E_g''	E_u''	$^1/_6\|\langle E_g''\|\|m^{e_u}\|\|E_u''\rangle\|^2$	$-g_\parallel(E_g'')/2$
	z-Polarized Transitions		
E_g'	E_u'	$^1/_6\|\langle E_g'\|\|m^{a_{2u}}\|\|E_u'\rangle\|^2$	0
E_g''	E_u''	$^1/_6\|\langle E_g''\|\|m^{a_{2u}}\|\|E_u''\rangle\|^2$	0

[a] $\langle A\|\|m^f\|\|J\rangle$ is a reduced electric-dipole transition moment for transition A → J. [b] $g_\parallel(E_g) = 2\langle E_g\alpha|L_0 + 2S_0|E_g\alpha\rangle = -2\langle E_g\beta|L_0 + 2S_0|E_g\beta\rangle$ with E_g superscripted with a ′ or ″ as appropriate.

All of the states with which we will be concerned arise from configurations $e_g^{n_e}\phi_1^1\phi_2^1$, where ϕ_1 and ϕ_2 are nondegenerate orbitals and n_e is the occupancy of the e_g orbital. For these configurations the orbital angular momentum is due purely to the e_g electrons, and one calculates (in units of $\hbar$)

$$\langle({}^4hM_S\theta)t\tau|L_0|({}^4hM_S\theta)t\tau\rangle = \theta(-1)^{n_b} \quad (17)$$

$$\langle({}^4hM_s\theta)t\tau|S_0|({}^4hM_S\theta)t\tau\rangle = M_S \quad (18)$$

The exponent n_b is the total number of unpaired electrons residing in b_1 or b_2 orbitals, and in eq 17 (and 19 and 20 below), θ is literally assigned the numerical value ±1 for the corresponding E irrep partner and zero for any one-dimensional irrep.

The first-order SO energy is

$$E_{SO}[({}^4hM_S\theta)t\tau] = \langle({}^4hM_S\theta)t\tau|\sum_k \xi_k s(k)\cdot l(k)|({}^4hM_S\theta)t\tau\rangle = \theta(-1)^{(n_e-1)/2}(-1)^{n_b}M_S\zeta_e/3 \quad (19)$$

where the sum over k includes all electrons in unfilled shells. The one-electron operators $s(k)$, $l(k)$, and ξ_k respectively pertain to the spin, orbital angular momentum, and SO interaction of electron k. ζ_e is an empirical SO coupling constant for an e_g electron, formally representing the radial integral of ξ_e. The factor $(-1)^{(n_e-1)/2}$ accounts for the inversion of the SO energy levels that occurs when the e_g orbital is more than half-filled. (Note that when $n_e = 2$, there is no first-order spin–orbit coupling.)

The first-order Zeeman energy of a molecule is dependent on its orientation relative to the magnetic field. In section IV.4, evidence is presented to show that the MnPc molecules are strongly oriented with their symmetry axes along the field direction. In the meantime, and for simplicity, we assume this to be the case. Equations 17 and 18 then give,

$$E_{Zeeman}[({}^4hM_S\theta)t\tau] = \mu_B B\langle({}^4hM_S\theta)t\tau|L_0 + 2S_0|({}^4hM_S\theta)t\tau\rangle = \mu_B B[\theta(-1)^{n_b} + 2M_S] \quad (20)$$

2. The ${}^4A_{2g}$ Ground-State Case. We assume a ${}^4A_{2g}$ term that arises from the configuration $b_{2g}^2e_g^2a_{1g}$,[13-17] which we abbreviate as $e_g^2a_{1g}$ in the following. In the D_{4h} double group this comprises two Kramers doublets, which correspond to $M_S = \pm{}^3/_2$ and $M_S = \pm{}^1/_2$, and transform respectively as E_g'' and E_g'. In the absence of orbital angular momentum, there is no first-order SO splitting, and the doublets are assumed degenerate in the absence of an external field (Figure 4). (Higher-order SO effects will give rise to a small zero-field splitting[35] which is irrelevant to the following

(34) Lever, A. B. P.; Licoccia, S.; Magnell, K.; Minor, P. C.; Ramaswamy, B. S. In *Electrochemical and Spectrochemical Studies of Biological Redox Components*; Kadish, K. M., Ed.; American Chemical Society: Washington, DC, 1982; pp 237–252.

(35) Harris, G. *Theor. Chim. Acta* **1968**, *10*, 119–154.

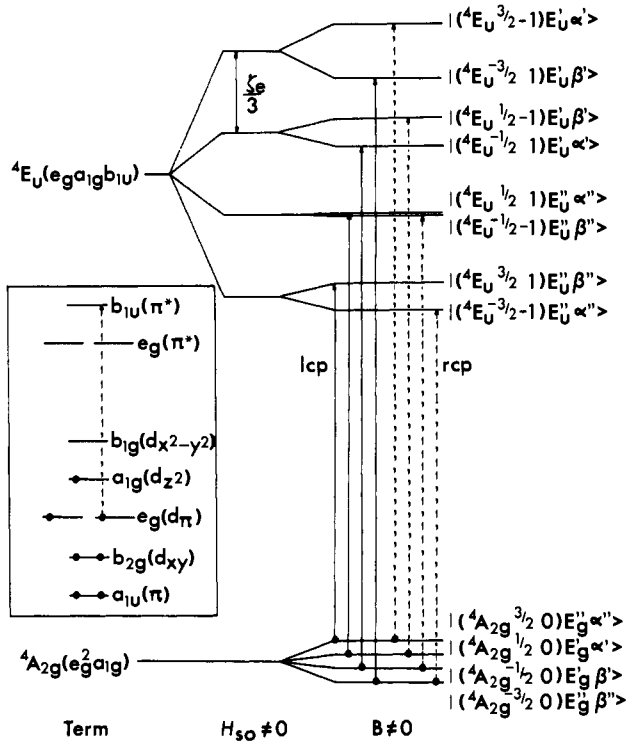

Figure 4. Energy level diagram for the transitions $^4A_{2g}(e_g^2a_{1g}) \rightarrow {}^4E_u(e_ga_{1g}b_{1u})$. The single-electron excitation, designated MLCT2,[10,34] is shown in the inset. The ordering of the orbital energies is that assumed by earlier workers to explain the magnetic behavior of β-MnPc crystals.[12-16] The Zeeman splittings shown on the right-hand side of the diagram are highly exaggerated in comparison with the spin–orbit energies. Left circularly polarized (lcp) and right circularly polarized (rcp) transitions are shown by solid and broken lines, respectively.

arguments, as will be demonstrated below.)

The only x,y-polarized spin-allowed transitions are of the type $^4A_{2g} \rightarrow {}^4E_u$. These can arise from $\pi \rightarrow \pi^*$ or CT transitions, but the general treatment is independent of the specific process. We choose the metal-to-ligand CT excitation $e_g(d_\pi) \rightarrow b_{1u}(\pi^*)$ (designated MLCT2 by Lever and co-workers[10,34]) as an illustration (Figure 4).

The $^4E_u(e_ga_{1g}b_{1u})$ excited term is split by first-order SO interactions into four Kramers doublets equally spaced by $\zeta_e/3$ (eq 19). Each of these doublets can be split only by an externally applied magnetic field (eq 20). (For the states $|(^4E_u \pm {}^1/_2 \pm 1)E_u''>$, the orbital and spin contributions to E_{Zeeman} cancel within the approximation $g_e \approx 2.0$, and hence the Zeeman splitting is small.) The splittings of the ground- and excited-state manifolds to first-order are shown in Figure 4. The circularly polarized transitions are also indicated. (lcp transitions are shown as full lines and rcp transitions as broken lines.)

With the approximations above, the total dipole strength for $^4A_{2g} \rightarrow {}^4E_u$ is

$$\bar{\mathcal{D}}_0(^4A_{2g}(e_g^2a_{1g}) \rightarrow {}^4E_u(e_ga_{1g}b_{1u})) = {}^2/_3|\langle e_g||m^{e_u}||b_{1u}\rangle|^2 \qquad (21)$$

where $\langle e_g||m^{e_u}||b_{1u}\rangle$ is the reduced electric-dipole transition moment for the excitation $e_g \rightarrow b_{1u}$. The intensity is found to divide equally among all of the possible transitions. The $\bar{\mathcal{C}}_0/\bar{\mathcal{D}}_0$ ratios in Table II are therefore directly comparable, and the total $\mathcal{C}$-term intensity integrated over the complete envelope of the transitions must be zero. This can also be seen from Figure 4. Each occupied level of the ground-state manifold will contribute equally to both a positive (lcp) and a negative (rcp) transition whose contributions to the integrated intensity of the MCD will cancel.

In the limit that observed band widths are very much greater than Zeeman energies (~1000 cm^{-1} versus ~1.0 cm^{-1} for the data in Figure 2), the fact that $\mathcal{C}$ terms can contribute at all to the MCD of a $^4A_{2g} \rightarrow {}^4E_u$ transition is entirely due to SO splitting of the excited state. To see this more clearly, consider the situation shown in Figure 4. At very low temperatures ($kT \lesssim \mu_B B$), the lowest-energy state, $|(^4A_{2g} - {}^3/_2 0)E''\beta''>$, will have a population in excess of other levels within the $^4A_{2g}$ manifold. The MCD should therefore include a strong, positive $\mathcal{C}$ term due to the transition terminating in $|(^4E_u \pm {}^3/_2 \mp 1)E_u'>$, and an equally strong, negative $\mathcal{C}$ term, due to the transition terminating in $|(^4E_u \pm {}^3/_2 \pm 1)E_u''>$. These will be separated by ζ_e, which in this case is the SO coupling constant for an $e_g(d_\pi)$ electron. For Mn, $\zeta_{3d} \sim 300$ cm^{-1},[36] which will be sufficient to partially resolve the opposed $\mathcal{C}$ terms. Hence we would expect the MCD to be bisignated, being negative at lower energy and positive at higher energy.

This qualitative result is independent of the specific excitation that is considered, though the sense of the bisignated $\mathcal{C}$ term may change. For example, for the ligand-to-metal CT excitation $a_{1u}(\pi) \rightarrow e_g(\pi)$ (designated LMCT1[10,34]), the excited-state manifold $^4E_u(a_{1u}e_g^3a_{1g})$ behaves in a very similar manner to that shown in Figure 4, except that the Zeeman splittings are somewhat different owing to the absence of unpaired b electrons. The situation is not changed for $\pi \rightarrow \pi^*$ transitions either. For example, for the Q excitation ($a_{1u}(\pi) \rightarrow e_g(\pi^*)$) the most important difference is that ζ_e now pertains to an $e_g(\pi^*)$ electron; hence the SO levels will be closer together and the resultant bisignated $\mathcal{C}$ term will be much weaker. The result is also independent of the finer details of the system. For example, if we allow higher-order SO splitting of $^4A_{2g}$, the same arguments as above can be applied within each Kramers doublet.

The crucial point is that single-signed $\mathcal{C}$ terms of the type observed near ~15000 cm^{-1} cannot be explained if the ground-state term is assumed to be $^4A_{2g}$. In fact, we can generalize further and state that single-signed $\mathcal{C}$ terms *cannot* be observed if the ground state is orbitally nondegenerate.

3. The ^4E_g Ground-State Case. We consider the case of a ^4E_g term that arises from the configuration $e_g^3a_{1g}b_{2g}$.[18,19] This term is split by first-order SO coupling into four Kramers doublets which are successively separated by intervals of $\zeta_e/3$ (Figure 5). Allowed x,y-polarized transitions are of the type $^4E_g \rightarrow {}^4A_{iu}$, $^4B_{iu}$, where $i = 1$ or 2.

Again we first consider the MLCT2 excitation ($e_g(d_\pi) \rightarrow b_{1u}(\pi^*)$). The excited-state configuration ($e_g^2a_{1g}b_{2g}b_{1u}$) gives rise to four quartet terms, $^4A_{1u}$, $^4A_{2u}$, $^4B_{1u}$, and $^4B_{2u}$, each of which has zero orbital angular momentum and hence cannot be split by first-order SO coupling. The treatment for the transitions $^4E_g \rightarrow {}^4A_{iu}$ or $^4B_{iu}$ is independent of the value of i and we show generalized cases in Figure 5. (Again we ignore higher-order SO and Zeeman effects.)

ζ_e is sufficiently large that for $T \sim 5$ K we need only consider the lowest SO level. For this reason, only the circularly polarized transitions from the Zeeman-split levels of $|(^4E_g \pm {}^3/_2 \mp 1)E_g'>$ are shown in Figure 5. (All other allowed transitions can be determined from Table I and the selection rule $\Delta M_S = 0$.) From eq 16–18,

$$g_\parallel \equiv g_\parallel((^4E_g \pm {}^3/_2 \mp 1)E_g') = 8 \qquad (22)$$

Using Table II and Figure 5, we would therefore expect $^4E_g(e_g^3a_{1g}b_{2g}) \rightarrow {}^4A_{iu}(e_g^2a_{1g}b_{2g}b_{1u})$ to be associated with negative $\mathcal{C}$ terms, and $^4E_g(e_g^3a_{1g}b_{2g}) \rightarrow {}^4B_{iu}(e_g^2a_{1g}b_{2g}b_{1u})$ to be associated with positive $\mathcal{C}$ terms.

As for the $^4A_{2g}$ ground-state term, the individual transitions shown in Figure 5 have equal dipole strengths with our approximations, and the total $\mathcal{C}$-term intensity summed over all levels of the excited-state manifold is zero. If the energy differences between excited-state levels (designated Δ in Figure 5) are small, then bisignated $\mathcal{C}$ terms will occur. However, these splittings are now dominated by electrostatic rather than SO effects and can easily be ~10000 cm^{-1},[36] in which case well-separated pairs of positive and negative $\mathcal{C}$ terms will arise.

In addition, it is not necessary to assume large Δ values for excitations such as MLCT2 to account for single-signed $\mathcal{C}$ terms.

(36) Griffith, J. S. *The Theory of Transition Metal Ions*; Cambridge University Press: Cambridge, 1961.

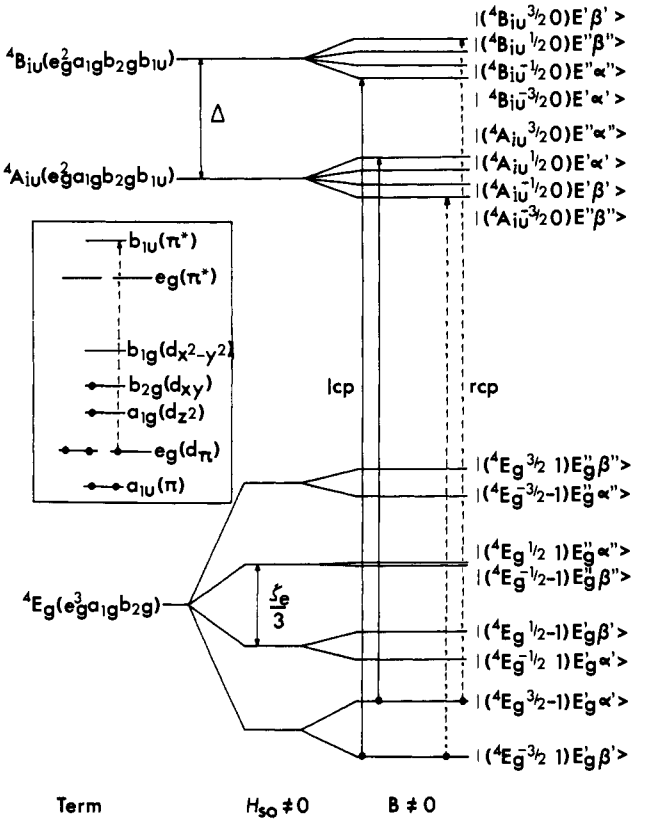

Figure 5. Energy level diagram for the transitions $^4E_g(e_g^3b_{2g}a_{1g}) \rightarrow {}^4A_{iu}(e_g^2b_{2g}a_{1g}b_{1u})$, $^4B_{iu}(e_g^2b_{2g}a_{1g}b_{1u})$ where $i = 1, 2$. The single-electron excitation, designated MLCT2,[10,34] is shown in the inset. The ordering of the orbital energies is that determined theoretically by earlier workers.[18,19] Δ represents the energy difference between the excited-state terms (section IV.3). The Zeeman splittings on the right-hand side of the diagram are highly exaggerated. Only the transitions from the lowest-lying Kramers doublet are illustrated. Left circularly polarized (lcp) and right circularly polarized (rcp) transitions are shown by solid and broken lines, respectively.

Ligand (a_{iu},b_{iu})-to-metal CT transitions that terminate in the $e_g(d_\pi)$ orbital each give rise to a single quartet excited-state term, which is orbitally nondegenerate and hence associated with a single-signed $\mathcal{C}$ term. For example, the excitation LMCT1 has a $^4B_{2u}(a_{1u}a_{1g}b_{2g})$ excited-state term, which will be associated with a positive $\mathcal{C}$ term. Similar excitations originating from b_{iu} ligand orbitals will give negative $\mathcal{C}$ terms.

Finally, $\pi \rightarrow \pi^*$ excitations will give rise to several quartet terms, but the Δ values will be very small since the metal orbitals are, to a first approximation, unaffected by the excitation. Hence we expect $\pi \rightarrow \pi^*$ transitions to be associated with weak bisignated $\mathcal{C}$ terms.

The predictions above are entirely consistent with the experimental data (Figure 2), where both single-signed and bisignated $\mathcal{C}$ terms are observed. The latter vary from being strong relative to the absorption (e.g., ~11 600 cm^{-1}, first solid arrow Figure 2), to being very weak (e.g., ~16 500 cm^{-1}, second solid arrow). We therefore conclude that the ground state of the isolated MnPc molecule arises from a ^4E_g term, in agreement with the calculated result.[18,19]

4. $g_\parallel$ and Molecular Orientation. Moment analysis can be applied to the data in Figure 2 to determine the value of $g_\parallel$ and so enable a quantitative comparison with eq 22. To obtain meaningful results, the integrations in eq 5 must be carried out over well-separated bands, and for this reason we expect the best estimate to be obtained from analysis of the intense, single-signed band at ~15 000 cm^{-1}. Assuming $T = 5$ K, we obtain $\mathcal{C}_0/\mathcal{D}_0 = 7.5$. The estimated uncertainty is ~20%, which arises predominantly from uncertainty in T but also includes errors in the CD calibration and choice of absorption base line. For the cases of completely random or completely preferential orientation respectively, this result gives $g_\parallel$ values of 15 ± 3 (Table II) or 7.5 ± 1.5 (eq 13).

These values can be independently checked by considering the saturation of the MCD as the field strength is increased.[32,37] For randomly oriented molecules, the equation appropriate to the transitions shown in Figure 5 is,[37]

$$\Delta A = K\int_0^1 \cos\Theta \tanh(\cos\Theta\, g_\parallel \mu_B B/2kT)\, d\cos\Theta \qquad (23)$$

where K is a constant and Θ is the angle between the molecular symmetry axis and the field direction. For the oriented case, cos Θ = 1 and

$$\Delta A = K \tanh(g_\parallel \mu_B B/2kT) \qquad (24)$$

Figure 3 shows the data for the weak positive band at ~18 760 cm^{-1} (indicated by an open boxed arrow in Figure 2) plotted against the ratio $\mu_B B/2kT$. This band was chosen since the MCD amplitude is relatively small ($\Delta A \lesssim 0.1$) over the range of field employed (0–3 T), thus avoiding errors of the kind mentioned in section III. The $g_\parallel$ value obtained by least-squares analysis of the data is dependent on the devation from linearity. It is independent of the absorption and unaffected by errors in the MCD scale calibration. The uncertainty arises almost entirely from the uncertainty in temperature, and hence the g value so obtained is more precise than that determined by moment analysis. Equations 23 and 24 give excellent and almost identical fits to the data (Figure 3), and with $T = 5.0 \pm 0.5$ K we obtain values for $g_\parallel$ of 11.3 ± 1.2 and 8.0 ± 0.8, respectively.

The $g_\parallel$ values obtained assuming random orientations are clearly unreasonable, while the values obtained assuming complete alignment of the molecular 4-fold axes with the field agree closely with that calculated for the $|(^4E_g \pm {}^3/_2 \mp 1)E_g'\rangle$ ground state. We therefore conclude that the MnPc molecules are highly oriented in the matrix with their z axes perpendicular to the surface of the deposition window and hence parallel to the applied magnetic field.

5. Spectral Assignments. Having demonstrated that the experimental data are both qualitatively and quantitatively consistent with a ^4E_g ground state, we now consider assignments of individual transitions. Lever and co-workers[10,34] have previously attempted this by correlating the absorption spectrum with redox potentials of MnPc solutions. (Although there are several potential problems with employing such correlations,[10] apart from the complications caused by axial ligation by the solvent molecules, they provide a convenient base from which to begin.) They predict three allowed CT transitions in the range of Figure 2: LMCT1 ($a_{1u}(\pi) \rightarrow e_g(d_\pi)$) at 10 970 cm^{-1}; LMCT2 ($a_{2u}(\pi) \rightarrow e_g(d_\pi)$) at 26 180 cm^{-1}; and MLCT2 ($e_g(d_\pi) \rightarrow b_{1u}(\pi^*)$) at 15 725 cm^{-1}.[34] (They also predict a further transition, MLCT1($e_g(d_\pi) \rightarrow e_g(\pi^*)$), but this is parity-forbidden and should be very weak or absent from the spectra even in the case of random molecular orientation.) We also anticipate the presence of $\pi \rightarrow \pi^*$ transitions due to the Q excitation ($a_{1u}(\pi) \rightarrow e_g(\pi^*)$) near 15 200 cm^{-1} and the B excitations (admixtures of $a_{1u}(\pi) \rightarrow e_g(\pi^*)$ and $a_{2u}(\pi) \rightarrow e_g(\pi^*)$) around 30 000 cm^{-1}.[8,24,38] Our assignments, as discussed now, are summarized in Table III and in Figure 2.

Starting at the high-energy end of Figure 2, a broad band is observed, centered at 29 600 cm^{-1}. The energy and general appearance of this band, along with the weakness of the corresponding MCD, strongly point to the assignment B($\pi \rightarrow \pi^*$).

LMCT1 and LMCT2 each give rise to a single quartet excited-state term: $^4B_{2u}(a_{1u}a_{1g}b_{2g})$ and $^4B_{1u}(a_{2u}a_{1g}b_{2g})$, respectively. In both cases we predict positive single-signed $\mathcal{C}$ terms, each with the same $\mathcal{C}_0/\mathcal{D}_0$ ratio. The most prominent positive $\mathcal{C}$ terms are at ~11 800, ~15 000, ~20 300, and ~28 200 cm^{-1}, but the first and third of these are components of bisignated features and cannot be associated with the LMCT transitions. We thus assign the bands at ~15 000 and ~28 200 cm^{-1} to LMCT1 and LMCT2,

(37) Schatz, P. N.; Mowery, R. L.; Krausz, E. R. *Mol. Phys.* **1978**, *35*, 1537–1557.
(38) Henriksson, A.; Roos, B.; Sundbom, M. *Theor. Chim. Acta* **1972**, *27*, 303–313.

Table III. Spectral Assignments for MnPc/Ar

excitation	$\mathcal{E}$/cm^{-1} predicted	$\mathcal{E}$/cm^{-1} observed	excited term	$\mathcal{C}_0/\mathcal{D}_0$ predicted[a]	$\mathcal{C}_0/\mathcal{D}_0$ observed
Q	15 200[b]	16 500	several	0[d]	~0[d]
B	30 000[b]	29 600	several	0[d]	~0[d]
LMCT1	10 970[c]	15 000	$^4B_{2u}$	8	7.5 ± 1.5
LMCT2	26 180[c]	28 200	$^4B_{1u}$	8	6.9 ± 3.0
MLCT2	15 725[c]	11 500	$^4A_{1u}$	−8	−6.9 ± 2.0
		11 800	$^4B_{1u}$	8	6.3 ± 2.0
		19 700	$^4A_{1u}$	−8	−3.1[e]
		20 300	$^4B_{1u}$	8	2.2[e]
CT (several)		21 400–25 000	several		−3.6[f]

[a] Predicted assuming a $^4E_g(e_g^3a_{1g}b_{2g})$ ground-state term and alignment of the symmetry axes of the MnPc molecules with the magnetic field (see text). [b] Predicted from transition energies of a selection of MPc molecules.[8] [c] Predicted from electrochemical data.[34] [d] Summed over all possible excited states. [e] These values represent gross underestimates due to strong mutual overlap (see text). [f] Summed over several overlapping transitions.

respectively (Figure 2), a few thousand cm^{-1} to the blue, but in reasonable agreement with their predicted energies (Table III). For LMCT1, moment analysis yields $\mathcal{C}_0/\mathcal{D}_0 = 7.5 \pm 1.5$. For LMCT2 the situation is complicated by strong overlap with the B band in the absorption spectrum. $\mathcal{C}_0$ was obtained by moment analysis since the zeroth MCD moment of the B band should be ≈0, but to obtain $\mathcal{D}_0$ it was necessary to resort to band fitting using a Gaussian line-shape function. From a two-band fit over the region 26 000–33 000 cm^{-1}, using the base line illustrated by the dashed line in Figure 2, we estimate $\mathcal{C}_0/\mathcal{D}_0 = 6.9 \pm 3.0$. (The larger error limits result from uncertainties inherent in the fitting procedure.) Thus the ratio is the same as for LMCT1 within our uncertainties.

A strong absorption band associated with weak bisignated MCD is expected in the vicinity of 15 000 cm^{-1} due to the Q($\pi \rightarrow \pi^*$) transitions. The band observed at almost exactly this energy is unambiguously assigned to a LMCT transition (see above), and we are forced to conclude that the Q band is at 16 500 cm^{-1}. This assignment stands against conventional wisdom, which has the Q band of MnPc in solution at significantly lower energy.[8] A value of 16 500 cm^{-1} is more in keeping with the Q band of the μ-oxo dimer, $Mn^{III}Pc$–O–$Mn^{III}Pc$.[4,5,8,39] However, we can discount the possibility of the presence of such a dimeric species in this work. Firstly, we have shown, both before and after deposition, that the material we used is unoxidized MnPc (section III); secondly, the temperature and field dependence of the MCD show that there is only one matrix-isolated species present; and finally, whereas the matrix-isolated species is clearly paramagnetic (giving rise to temperature dependent MCD), $Mn^{III}Pc$–O–$Mn^{III}Pc$ is diamagnetic with much weaker MCD than that associated with the 16 500-cm^{-1} band of Figure 2.[39]

For MLCT2, we predict four transitions, all with similar dipole strengths (section IV.3). Two should show positive $\mathcal{C}$ terms and two should show negative $\mathcal{C}$ terms, with the total $\mathcal{C}$-term intensity summing (approximately) to zero. The obvious candidates are the pairs of transitions corresponding to the bisignated $\mathcal{C}$ terms near 11 600 and 20 000 cm^{-1} (Figure 2), with the negative lobes corresponding to $^4A_{1u}$ excited states and the positive lobes to $^4B_{1u}$ excited states. The average energy of these transitions coincides almost exactly with the predicted energy of MLCT2 (Table III), and their relatively large separation can be accounted for by electrostatic effects. To illustrate the latter point, consider the octahedral parentage of the excited states, ignoring the effects of the $b_{1u}(\pi^*)$ electron. Treating the central metal as Mn(III)(d^4), the parent states derive from the terms $^5E(t_2^3e)$, $^3E(t_2^3e)$, $^3T_1(t_2^3e)$, and $^3T_2(t_2^3e)$, which span a range of energies $16B + 6C$.[36] For Mn(III), $B \sim 1\,140$ cm^{-1} and $C \sim 3\,675$ cm^{-1};[36] hence the observed separation of ~8 400 cm^{-1} is easily accounted for.

The two higher-energy MLCT2 transitions (~20 000 cm^{-1}) are sufficiently well separated to obtain reasonable results using moment analysis. In an attempt to partially account for their mutual overlap and overlap with negative $\mathcal{C}$ terms to the blue, a local MCD base line was chosen to pass through the inflection points (dotted line, Figure 2). This yields $\mathcal{C}_0/\mathcal{D}_0$ values of −6.9 ± 2.0 and 6.3 ± 2.0, somewhat lower than, but within experimental uncertainty of the predicted magnitudes for the $^4E_g(e_g^3a_{1g}b_{2g})$ ground-state term (Table III). The two lower-energy MLCT2 transitions (~11 600 cm^{-1}) overlap strongly, and we can find no objective means by which to obtain accurate estimates for their $\mathcal{C}_0/\mathcal{D}_0$ ratios. Applying moment analysis, arbitrarily choosing the zero-crossing of the MCD as the demarcation between the two transitions, we obtain −3.1 and 2.2. However, these must represent gross underestimates due to cancellation of the MCD in the region of overlap, and it would seem entirely reasonable to expect that the true values are near the predicted values of ±8.

Centered near 22 500 cm^{-1} is a strong, broad, asymmetric absorption band labeled "CT" (Figure 2). The MCD in this region is predominantly negative, with $\mathcal{C}_0/\mathcal{D}_0 \sim -3.6$. The low magnitude of $\mathcal{C}_0/\mathcal{D}_0$ in comparison with other bands and the fact that the dispersion of the MCD differs from that of the absorption suggest the presence of several overlapping transitions, some presumably associated with positive $\mathcal{C}$ terms. These must be CT transitions that were not predicted by Lever et al.[10,34] There are many ligand orbitals that could be involved in such transitions,[38] but we do not have sufficient information to be more specific.

Next, we comment on the several weak bands that are observed between the stronger transitions that we have assigned. Lever et al.[10] assign some of these, to the red of 15 000 cm^{-1}, to trip-multiplets. We think that it is as likely that most or all of the weak bands arise from vibrational overtones built on electronic origins.

Finally, we emphasize that these assignments should be regarded as being somewhat formal since various of these transitions are undoubtedly admixtures of several excitations, and many of the orbitals will be of mixed metal and ligand parentage. For example, the unexpectedly high energy of the Q band is probably a consequence of interactions between the π orbitals of the ligand and unfilled valence orbitals of the metal ion. In D_{4h}, the only orbitals of appropriate symmetry to take part in such mixing transform as e_g, and we suspect an appreciable $e_g(\pi^*)$–$e_g(d_\pi)$ interaction. This will tend to shift $e_g(\pi^*)$ to higher energy so that the Q transition (nominally $a_{2u}(\pi) \rightarrow e_g(\pi^*)$) is blue-shifted, while LMCT1 (nominally $a_{2u}(\pi) \rightarrow e_g(d_\pi)$) is red-shifted. As a secondary consequence, the intensity borrowing inherent in such an interaction leads to modifications of the dipole strengths of the transitions. Schaffer et al.,[18] using an extended Hückel calculation, predict such an interaction with the contributions of the metal d_π orbitals to $e_g(\pi^*)$ and $e_g(d_\pi)$ being 4.1% and 84.1%, respectively.

Mixing of orbitals may also be partially responsible for the sensitivity of the absorption spectrum of MnPc to the molecular environment (section I). The d_π orbitals of the metal (d_{xz} and d_{yz}) are susceptible to axial interactions, which could quench or enhance the π^*–d_π mixing, resulting in changes in the energies and relative intensities of the transitions. In the extreme, such effects, in combination with the change of crystal field, might destabilize the $a_{1g}(d_{z^2})$ and $e_g(d_\pi)$ orbitals sufficiently relative to $b_{2g}(d_{xy})$ to make the $b_{2g}^2e_g^2a_{1g}$ configuration more favorable. In support of this hypothesis, the molecular ground state seems likely to be different in two solid-state phases of MnPc. In the β-phase, where there is an axial interaction between Mn and the azamethine nitrogen atoms of adjacent molecules,[21,22] the ground-state term is $^4A_{2g}(b_{2g}^2e_g^2a_{1g})$.[13-17] In the α-phase, such interactions are absent,[40] and although the molecular ground state has not been determined, there is evidence that it is the same as for MnPc/Ar; the thin-film absorption spectrum of α-MnPc[4] is very similar to that of MnPc/Ar, except that the bands are broader and those assigned to CT transitions in this work are shifted several hundred cm^{-1} to the red.

V. Conclusions

The absorption and MCD of MnPc/Ar show unambiguously that the chromophore has an orbitally degenerate ground state,

(39) Wright, S.; Stillman, M. J. Unpublished results.

(40) Stymne, B.; Sauvage, F. X.; Wettermark, G. *Spectrochim. Acta* **1979**, *35A*, 1195–1201.

and our analysis is entirely consistent with the ground-state term assignment $^4E_g(e_g^3a_{1g}b_{2g})$. This conclusion is in disagreement with the results of magnetic measurements on the β-phase solid[13-17] which suggest a $^4A_{2g}(b_{2g}^2e_g^2a_{1g})$ ground-state term. The difference may be due to the fact that azamethine nitrogens of adjacent molecules lie above and below the Mn atoms in the β-phase.[21,22]

The dispersion of the MCD bands and correlations with earlier electrochemical data[10,34] have allowed us to formally assign the major bands in the electronic spectra. We are confident of our ability to distinguish between transitions that are principally of $\pi \rightarrow \pi^*$ or CT character, but more specific descriptions await a sophisticated quantum-mechanical calculation for both the ground and excited states.

The absorption spectrum of MnPc/Ar is quite different from earlier solution spectra,[3-5,8-11] a fact that may be attributable to axial ligation (with oxygen in some cases) and perhaps to a difference in ground state. Our results suggest that the strongest red band of the solution spectra contains contributions from both the $Q(\pi \rightarrow \pi^*)$ and LMCT1 excitations.

Acknowledgment. This work was supported by the National Science Foundation under Grants CHE8700754 and CHE8902456 and by the Natural Sciences and Engineering Research Council of Canada (to M.J.S.). One of us (M.E.B.) acknowledges partial support from the ONT/NRL Laser Block Program. We acknowledge the assistance of Z. Gasyna and R. J. Van Hale with some of the experimental work.

Registry No. MnPc, 14325-24-7.

Pentaenyl Cations from the Photolysis of Retinyl Acetate. Solvent Effects on the Leaving Group Ability and Relative Nucleophilicities: An Unequivocal and Quantitative Demonstration of the Importance of Hydrogen Bonding

Norbert J. Pienta* and Robert J. Kessler

Contribution from the Department of Chemistry, CB# 3290, University of North Carolina, Chapel Hill, North Carolina 27599-3290. *Received June 12, 1991*

Abstract: The photolysis of retinyl acetate leads to carbon-oxygen bond heterolysis and yields the retinyl cation within 100 ps. This pentaenyl cation, which has an absorbance centered at 590 nm, is observed using picosecond and nanosecond laser transient absorption. This provides access to ion dynamics and affords the opportunity to study aspects of the S_N1 mechanism, including the effect of hydrogen bonding cosolvents like water and alcohols. Contact ion pairs appear to be important in the early time regime, but free ions are the reactive species in polar solvents in the nanosecond experiment. Trapping of the free ions with nucleophiles yields a collection of rate data from Stern-Volmer quenching which in turn gives linear plots versus Pearson/Swain-Scott n values, measures of relative nucleophilicity based on S_N2 reactions. These linear plots show a marked dependence on water content in the solvent acetonitrile with an increase in selectivity (i.e., slope of the line) with added water. For example, the second order rate constant for reaction of the retinyl cation with fluoride decreases by over four orders of magnitude in changing the solvent from dry acetonitrile to the same solvent with 11 M water. This is interpreted to be the result of hydrogen bonding between water and the nucleophiles. The special salt effect of Li^+ is also demonstrated to arise from the strong interaction of this Lewis acid and the nucleophiles.

Introduction

Reactions of carbenium ions with nucleophiles have been studied extensively, and recent work includes the use of laser flash photolysis to measure rate constants directly.[1] Other sources of absolute rate constants come from reactions of very stable cations using rapid mixing techniques and include studies by Ritchie[2] and Bunton.[3] A comprehensive picture is beginning to emerge and, for example, includes models for the relationship between solvolytic reactivity and nucleophile selectivity[4] and for the coordination of carbanions with carbenium ions.[5] In spite of these efforts and despite implications of the importance of hydrogen bonding,[1a,6,7]

(1) (a) McClelland, R. A.; Kanagasabapathy, V. M.; Banait, N. S.; Steenken, S. *J. Am. Chem. Soc.* **1991**, *113*, 1009-14. (b) McClelland, R. A.; Banait, N. S.; Steenken, S. *J. Am. Chem. Soc.* **1989**, *111*, 2929-35. (c) *J. Am. Chem. Soc.* **1986**, *108*, 7023-27. (d) McClelland, R. A.; Kanagasabapathy, V. M.; Steenken, S. *J. Am. Chem. Soc.* **1988**, *110*, 6913-4. (e) McClelland, R. A.; Kanagasabapathy, V. M.; Banait, N. S.; Steenken, S. *J. Am. Chem. Soc.* **1989**, *111*, 3966-72. (f) Steenken, S.; McClelland, R. A. *J. Am. Chem. Soc.* **1989**, *111*, 4967-73. (g) Faria, J. L.; Steenken, S. *J. Am. Chem. Soc.* **1990**, *112*, 1277-9. (h) McClelland, R. A.; Mithavanan, N.; Steenken, S. *J. Am. Chem. Soc.* **1990**, *112*, 4857-61. (i) Bartl, J.; Steenken, S.; Mayr, H.; McClelland, R. A. *J. Am. Chem. Soc.* **1990**, *112*, 6918-28. (j) McClelland, R. A.; Cozens, F.; Steenken, S. *Tetrahedron Lett.* **1990**, 2821-24. (k) Schnabel, W.; Naito, I.; Kitamura, T.; Kobayashi, S.; Taniguchi, H. *Tetrahedron* **1980**, *36*, 3229-31. (l) Kobayashi, S.; Kitamura, T.; Taniguchi, H.; Schnabel, W. *Chem. Lett.* **1983**, 1117-20. (m) Van Ginkel, F. I. M.; Visser, R. J.; Varma, C. A. G. O.; Lodder, G. *J. Photochem.* **1985**, *30*, 453-73. (n) Kobayashi, S.; Zhu, Q. Q.; Schnabel, W. *Z. Naturforsch.* **1988**, *43B*, 825-9. (o) Minto, R. E.; Das, P. K. *J. Am. Chem. Soc.* **1989**, *111*, 8858-66. (p) Johnston, L. J.; Lobaugh, J.; Wintgens, V. *J. Phys. Chem.* **1989**, *93*, 7370-4. (q) Alonso, E. O.; Johnston, L. J.; Scaiano, J. C.; Toscano, V. G. *J. Am. Chem. Soc.* **1990**, *112*, 1270-1.

(2) (a) Ritchie, C. D. In *Nucleophilicity*; Harris, J. M., McManus, S. P., Eds.; Advances in Chemistry Series 215; American Chemical Society: Washington, DC, 1987; pp 169-79. (b) Ritchie, C. D.; Hofelich, T. C. *J. Am. Chem. Soc.* **1980**, *102*, 7039-44. (c) Ritchie, C. D.; Gandler, J.; *J. Am. Chem. Soc.* **1979**, *101*, 7318-23. (d) Ritchie, C. D. *Acc. Chem. Res.* **1972**, *5*, 348-54, and references cited therein.

(3) (a) Bunton, C. A.; Paik, C. H. *J. Org. Chem.* **1976**, *41*, 40-4. (b) Bunton, C. A.; Huang, S. K. *J. Am. Chem. Soc.* **1973**, *95*, 2701-2. (c) *J. Am. Chem. Soc.* **1974**, *96*, 515-22; **1972**, *94*, 3536-44.

(4) Ta-Shma, R.; Rappoport, Z. *J. Am. Chem. Soc.* **1983**, *105*, 6082-95.

(5) (a) Arnett, E. M.; Amarnath, K.; Harvey, N. G.; Cheng, J. P. *J. Am. Chem. Soc.* **1990**, *112*, 344-55. (b) Arnett, E. M.; Molter, K. E. *Acc. Chem. Res.* **1985**, *18*, 339-46, and references cited therein.

(6) (a) Reichardt, Chr. *Solvents and Solvent Effects in Organic Chemistry*, 2nd ed.; VCH: New York, 1990, pp 208-283, and references cited therein. (b) Epshtein, E. P. *Russian Chem. Rev.* **1979**, *48*, 854. (c) Okamoto, K. *Pure Appl. Chem.* **1984**, *56*, 1797. (d) Parker, A. J. *Chem. Soc. Quart. Rev.* **1962**, *16*, 163. (e) Parker, A. J. *Adv. Phys. Org. Chem.* **1968**, *5*, 173-235.

0002-7863/92/1514-2419$03.00/0